THE ASTROPHYSICAL JOURNAL, 484:118–130, 1997 July 20

A DRAMATIC MILLIMETER WAVELENGTH FLARE IN THE GAMMA-RAY BLAZAR NRAO 530

GEOFFREY C. BOWER, DONALD C. BACKER, MELVYN WRIGHT, AND JAMES R. FORSTER
Radio Astronomy Laboratory, University of California, Berkeley, CA 94720

AND

HUGH D. ALLER AND MARGO F. ALLER
Astronomy Department, University of Michigan, Dennison Building, Ann Arbor, MI 48109-1090
Received 1996 September 17; accepted 1997 February 21

ABSTRACT

We present 3 mm wavelength VLBI observations and up to 30 yr of monitoring at radio through submillimeter wavelengths of the gamma-ray blazar NRAO 530. We discuss the dramatic flare that tripled the millimeter wavelength flux in 1994 and 1995 following three decades of increasing activity. VLBI observations during the flare show the creation of new components in a bent jet on subparsec scales. The components move at an apparent velocity of 7*c*. The observations also imply expansion in a separate component with a speed greater than 26*c*. We apply synchrotron self-Compton models to the core and jet to determine magnetic field strengths, particle densities, and Doppler boosting factors. We are unable to provide a satisfactory physical explanation for the high apparent velocity component.

The increase in millimeter and radio wavelength fluxes is correlated with a rise in the gamma-ray flux detected by EGRET. We show that gamma-ray detections do not always occur during or immediately prior to a millimeter wavelength flare, contrary to assertions in the literature. We associate the VLBI component creation with the gamma-ray activity, although not with a specific flare.

We consider what may distinguish gamma-ray blazars from other variable, flat-spectrum radio objects. Our data strengthen the correlation between superluminal motion and gamma-ray emission in blazars. The distribution of jet misalignment angle for 28 EGRET sources, determined from a survey of the literature, does not differ significantly from that of other blazars. This suggests that the geometries of gamma-ray blazars do not differ from those of gamma-ray–quiet blazars on the scales sampled by VLBI.

Subject headings: galaxies: jets — gamma rays: observations — radiation mechanisms: nonthermal — radio continuum: galaxies

1. INTRODUCTION

Gamma-ray blazars have been identified as a distinct class of object through observations of the Energetic Gamma Ray Experiment Telescope (EGRET) on the *Compton Gamma Ray Observatory* (von Montigny et al. 1995a). Their properties include intense and variable emission at energies exceeding 100 MeV, a variable flat radio spectrum, superluminal motion in the radio core, and optical polarization. These properties are believed to be heavily influenced by relativistic beaming in a narrow jet with near light speed velocities directed at a small angle to the line of sight. A principal issue in the study of these objects is the identification of properties that uniquely separate gamma-ray–loud from gamma-ray–quiet blazars. Gamma-ray emission has not been detected from a substantial fraction of blazars not otherwise differentiable from gamma-ray blazars (von Montigny et al. 1995b). Temporal variability or differential beaming for the gamma-ray and radio emission are possible explanations for this division.

Millimeter wavelength very long baseline interferometry (VLBI) provides a unique tool for probing the dynamics and physical conditions of these jets. The superior resolution at short wavelengths allows precise imaging of an active nucleus rapidly following the creation of new components in the jet. Furthermore, synchrotron radiation, the emission from relativistic electrons in a magnetic field and the source of the radio emission in blazars, becomes optically thin in blazars at wavelengths between 1 cm and 1 mm (Stevens et al. 1994). The low opacity permits a deeper view into the radio core. Marscher (1995), for example, has shown that sensitive imaging at optically thin wavelengths is capable of discriminating between a variety of models for gamma-ray emission. Finally, the shorter lifetime of synchrotron sources at millimeter wavelengths allows improved temporal resolution of flares.

We note that an intimate connection appears to exist between millimeter VLBI and EGRET sources. Nine of the 30 blazars detected with 3 mm wavelength VLBI (Rogers 1994), including five of the 10 brightest, are also EGRET sources (Thompson et al. 1995). This is in contrast to the EGRET detection of 51 sources from the 518 in the Kühr et al. (1981) all-sky $S(5\ \mathrm{GHz}) \geq 1$ Jy catalog. This is an expected consequence of the flat-spectrum character of EGRET sources (e.g., von Montigny et al. 1995a).

The interpretation of millimeter VLBI observations is sharpened with the inclusion of flux density and polarization monitoring at all wavelengths. Zhang et al. (1994) present a synchrotron self-Compton analysis of the gamma-ray blazar 0528+134 based on 8 and 22 GHz VLBI and concurrent *ROSAT* and radio frequency monitoring. Prevailing theories of blazars (e.g., Königl 1981; Marscher & Gear 1985; Sikora, Begelman, & Rees 1994) and compilations of broadband spectra (e.g., von Montigny et al. 1995a) typically identify two or three dominant emission mechanisms in distinct bands: synchrotron radiation peaking in radio through infrared wavelengths, thermal

radiation from a disk peaking in optical through X-ray wavelengths, and high-energy emission scattered through the inverse-Compton process from either synchrotron or thermal sources. Activity is expected to be correlated over broad ranges of the spectrum. In one model, for example, a synchrotron flare might occur in the optical band. Shortly thereafter, relativistic electrons will scatter the synchrotron photons into gamma rays. As the synchrotron source cools radiatively, the synchrotron flare will propagate to lower frequencies. The flare's appearance at all frequencies depends on its environment; a flare may be delayed or hidden if the optical depth is large.

Studies have found mixed evidence for correlated activity in radio through optical wavelengths (e.g., Tornikoski et al. 1994; Stevens et al. 1994). Gamma-ray activity was found to be correlated with infrared to X-ray activity in 3C 279 (Maraschi et al. 1994) and to occur before or during a rise in radio and millimeter flux in many sources (Reich et al. 1993; Valtaoja & Teräsranta 1995).

We present here 3 mm wavelength VLBI observations of the blazar NRAO 530 along with flux density monitoring at radio through submillimeter wavelengths. NRAO 530 is a $m_{pg} \approx 18.5$ mag QSO (Welch & Spinrad 1973) with a redshift $z = 0.902$ (Junkkarinen 1984). It is renowned for its flat spectrum from 80 MHz to 100 GHz (NASA Extragalactic Database). NRAO 530 is identified with EGRET source 2EG 1735−1312 (Thompson et al. 1995). The bolometric luminosity, which is dominated by the high-energy emission, is $0.9 \times 10^{48}\ h^{-2}$ ergs s^{-1}, assuming isotropic emission (Nolan et al. 1996). Throughout this paper we assume $q_0 = 0.5$ and $H_0 = 100\ h$ km s^{-1} Mpc^{-1}. This implies an angular to linear scale conversion of $4.2\ h^{-1}$ pc mas^{-1} and a luminosity distance of $3.1\ h^{-1}$ Gpc.

NRAO 530 underwent a dramatic millimeter and radio wavelength flare beginning in 1994. In § 2, we analyze the radio flux history to show that the recent flare is a unique event in this object's history. The flare follows a decades-long increase in activity. We also discuss the relationship between the radio frequency and the gamma-ray light curves. In § 3, we present millimeter VLBI observations of NRAO 530. In § 4, we examine the newly formed jet components with dynamical and physical models. We consider the relationship of centimeter wavelength polarization to the compact structure. Finally, we compare our results to other studies of gamma-ray blazars in § 5.

2. FLUX DENSITY MONITORING

2.1. *Observations*

Total flux density and polarization at 4.8, 8.0, and 14.5 GHz were obtained with the 26 m radio telescope of the University of Michigan following procedures outlined in Aller et al. (1985). Flux densities at 22 and 37 GHz obtained with the 13.7 m Metsahovi radio telescope with the standard ON-ON techniques are listed in Table 1. All observations are calibrated against DR 21. A more detailed description of the receiving system can be found in Teräsranta et al. (1992).

Flux density measurements were made with the Berkeley-Illinois-Maryland Association Array at Hat Creek Radio Observatory between 83.0 and 111.9 GHz, but chiefly between 83.0 and 90.4 GHz. We will refer to the frequency of these observations as 90 GHz throughout the paper. Some of the variability seen in the data is due to the range of frequencies. The data were taken principally for phase calibration in a variety of observing programs. Data were calibrated with concurrent observations of planets.

TABLE 1

FLUX DENSITY DATA

Frequency (GHz)	Date	Flux (Jy)	Error (Jy)	Source
22	1995 Jan 07	8.90	0.34	Metsahovi
	1995 Apr 15	11.18	0.47	Metsahovi
	1995 Apr 21	11.25	0.53	Metsahovi
37	1995 Apr 14	11.76	0.44	Metsahovi
	1995 Apr 20	10.94	0.43	Metsahovi
150.....	1995 May 10	7.09	0.35	JCMT
230.....	1994 Jun 25	2.6	0.2	SEST
	1994 Nov 11	5.5	1.0	OVRO
	1994 Nov 29	3.7	1.0	OVRO
	1994 Dec 21	3.9	1.0	OVRO
	1995 Feb 06	6.8	1.0	OVRO
	1995 Feb 06	9.5	1.0	OVRO
	1995 Feb 21	12.0	1.0	OVRO
	1995 Feb 24	8.0	1.0	OVRO
	1995 Apr 01	8.8	0.7	SEST
	1995 Apr 03	8.4	0.7	SEST
	1995 Apr 05	6.2	1.0	OVRO
	1995 Apr 05	6.7	1.0	OVRO
	1995 May 05	4.9	1.0	KP
	1995 May 10	5.83	0.30	JCMT
	1995 May 19	7.6	1.0	KP
	1995 May 20	6.3	1.0	KP
270.....	1995 May 10	5.66	0.30	JCMT
375.....	1995 May 10	4.67	0.47	JCMT

Additional millimeter and submillimeter data are summarized in Table 1. Flux densities at 150, 230, 270, and 375 GHz were taken with the ^{3}He-cooled facility bolometer, UKT14 (Duncan et al. 1990) at the 15 m James Clerk Maxwell Telescope (JCMT) (J. Stevens & I. Robson 1995, private communication). Calibration was made with respect to the planets and the JCMT secondary calibrators (Sandell 1994). The effects of atmospheric extinction were removed in the manner described by Stevens & Robson (1994). Flux densities at 230 GHz were also obtained with the NRAO 12 m telescope at Kitt Peak, the Swedish-ESO Submillimetre Telescope (SEST) (M. Tornikoski 1995, private communication), and the Owens Valley Radio Observatory (J. Carlstrom 1995, private communication). The Kitt Peak observations were calibrated by frequent sky tips and simultaneous observations of the planets Venus, Mars, Jupiter, and Uranus. The SEST observations followed procedures for data collection and analysis provided in Tornikoski et al. (1996).

2.2. *Light Curves at Radio Frequencies*

In Figure 1 we show the light curves of NRAO 530 at 4.8, 8.0, 14.5, and 90 GHz. The 8.0 GHz data show a long history of slowly increasing flux and activity that is mirrored in the shorter histories available at 4.8 and 14.5 GHz. The Hat Creek data show a history of relatively stable flux at 90 GHz until 1994. Fluctuations at 90 GHz have lower frequency counterparts, which propagate from 90 to 14.5 GHz with time delays of 0.5 yr or less. During flares, the 4.8 to 90 GHz spectrum was flat following the initial inverted-spectrum rise.

Some optical and centimeter wavelength activity appear to be unrelated. The optical monitoring data of Webb et al. (1988) include a $\sim$3 mag flare in 1977 that has no apparent

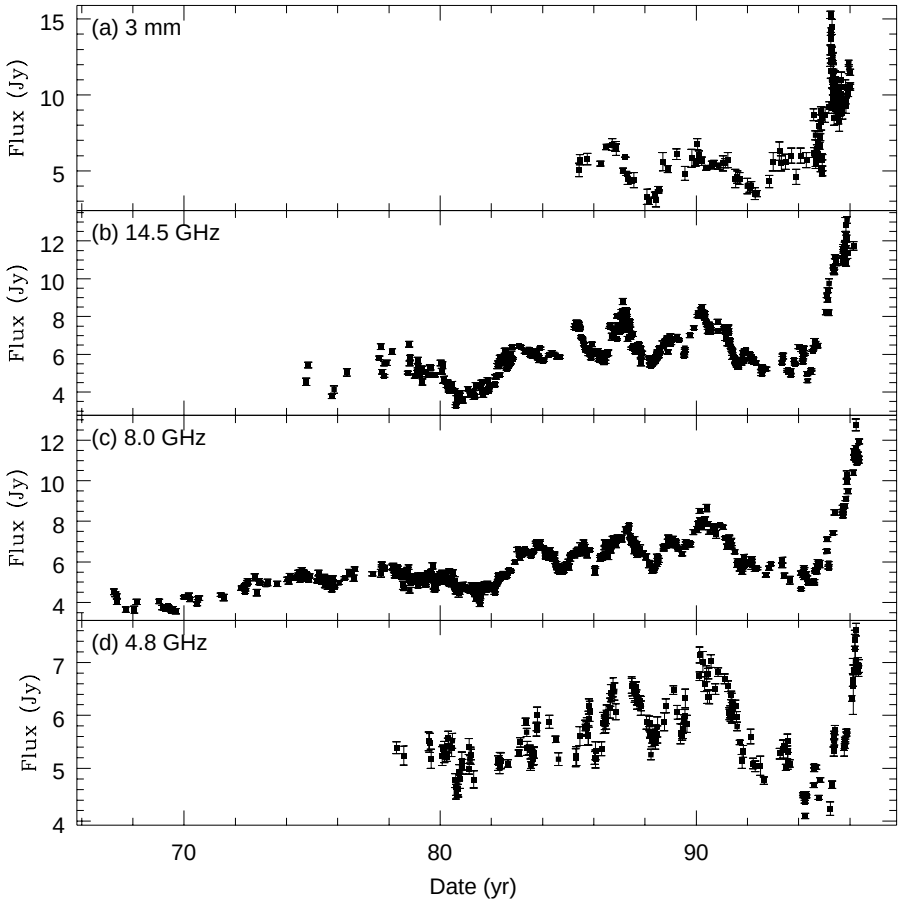

FIG. 1.—Flux histories at (*a*) 90 GHz from Hat Creek, (*b*) 14.5 GHz, (*c*) 8.0 GHz, and (*d*) 4.8 GHz from the University of Michigan

counterpart at centimeter wavelengths, where the flux declined for $\gtrsim 3$ yr before slowly increasing.

A very bright and apparently unique flare occurred in late 1994 and early 1995. The well-sampled centimeter wavelength fluxes preclude a similar event in the past 30 yr. Although the sparser sampling at 90 GHz allows the possibility of a rapid, undetected flare, the similarity between flux variations at millimeter and centimeter wavelengths argues against this.

We show in Figure 2 the light curves for NRAO 530 from 1991 to 1996 at 4.8, 8.0, 14.5, and 90 GHz. These light curves show a sharp tripling in the 90 GHz flux followed by rises in the flux at lower frequencies. We also include in Figure 2 the gamma-ray flux detected by EGRET in this figure (Mukherjee et al. 1997), which we discuss further in § 2.4.

2.3. *Spectral Evolution of the Flare*

For simplicity we adopt an analytic model of the quiescent spectrum: flat for $\nu < 130$ GHz at 4 Jy and declining as $\nu^{-0.5}$ for $\nu > 130$ GHz. The spectral break and the high-frequency spectrum spectral index depend primarily on the 1994 June 230 GHz observations. This model matches well the minimum values of the centimeter and millimeter fluxes within the past decade. However, it overpredicts the optical flux by a factor of 100, suggesting a further break in the spectrum in the submillimeter or infrared band.

We show the spectral evolution of the flare event from 1994 June through 1995 May in Figure 3. The millimeter and submillimeter wavelength fluxes in the spectra were obtained within 7 days of the given dates. The centimeter wavelength fluxes were interpolated between observations separated by as long as 2 months from the given date, although separations of 2 weeks or less are typical for observations in 1995.

During the time shown two distinct flares nearly tripled the 90 GHz flux. The state in 1994 June (A) is slightly elevated from the quiescent state. A sharp rise in flux began in late 1994 (B) and continued into early 1995 (C). The 90 GHz flux remained level into 1995 February (D). The second flare appeared at this time at 230 GHz (D and E) before propagating to 90 GHz (E and F). In stages F through H, the flare peaked at 90 GHz, reaching a maximum flux of 15 Jy. At the time of the VLBI experiment (1995.32), the 90 GHz flux had fallen to 12.5 Jy. Throughout this time and the remainder of 1995, the centimeter wavelength flux rose steadily. The flares are increasingly blended at longer wavelengths, but appear with time delays similar to those of the earlier, lower amplitude flares. Following the flare's peak and decline, the 90 GHz flux remained constant near 10 Jy.

2.4. *Gamma-Ray Activity*

EGRET reported increasing flux from the direction of NRAO 530 between 1991 and 1995 (Mukherjee et al. 1997). The average flux quadrupled in this period. For the periods 1991.5–1992.2, 1993.2–1993.7, 1994.2–1994.6, and 1995.4–1995.5, the average detected fluxes were 34 ± 16, 68 ± 19, 64 ± 26, and 127 ± 48 pJy, respectively. The errors represent the scatter in the measurements and are slightly larger than the errors in the mean. This may indicate vari-

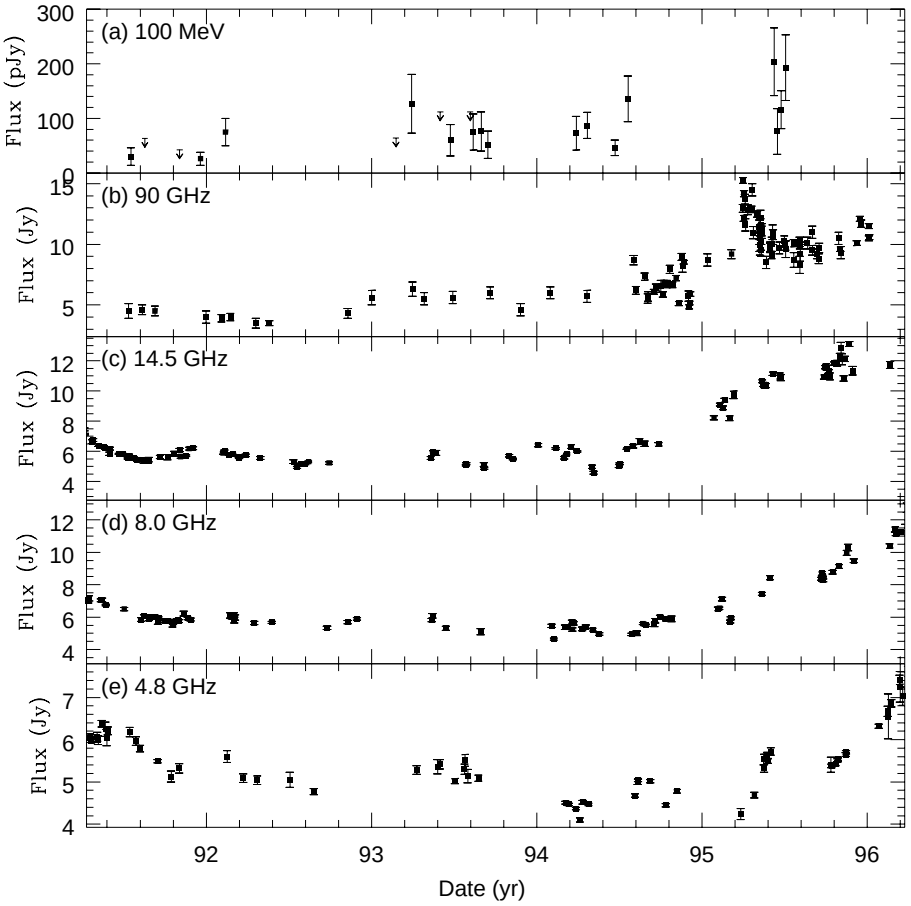

FIG. 2.—Flux histories at (*a*) 100 MeV from EGRET, (*b*) 90 GHz from Hat Creek, (*c*) 14.5 GHz, (*d*) 8.0 GHz, and (*e*) 4.8 GHz from the University of Michigan from 1991 to 1996.

able flux, i.e., flares, during the averaging periods. However, the evidence for flares is weak. The light curve is consistent with a monotonically increasing flux over the 4 yr of observation. Secular evolution of the flux in blazars has not been detected at gamma-ray or soft X-ray wavelengths (Giommi et al. 1990). The two brightest detections occurred in 1995 June, following the peak of the millimeter-wave flare.

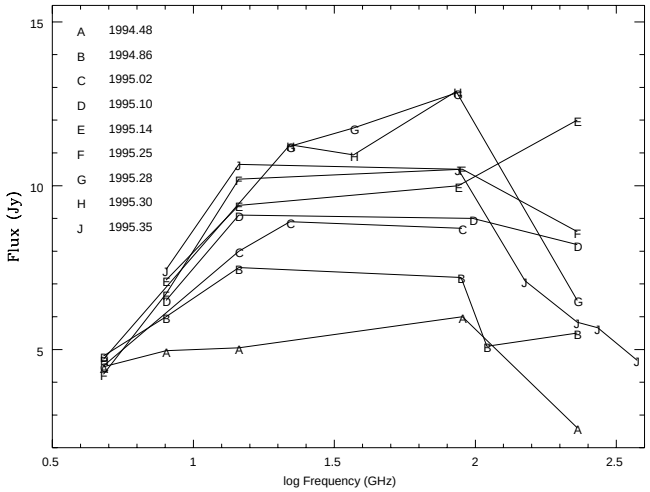

FIG. 3.—Spectral evolution from 1994 June through 1995 May. The letters follow a sequence of increasing date, as marked on the figure. See the text for details of spectral construction.

Many of the gamma-ray detections occur in times of declining or constant millimeter- and centimeter-wave flux. Even the brightest gamma-ray detections do not have obvious counterpart flares at the lower frequencies. This is contrary to the conclusions of Reich et al. (1993) and Valtaoja & Teräsranta (1995) that gamma-ray detections occur only at times of increasing or peaking radio/millimeter flux. This new conclusion results in part from a reanalysis of the EGRET data since the first EGRET catalog (Fichtel et al. 1994). Many upper limits in the first EGRET catalog have been reclassified as low signal-to-noise detections in Mukherjee et al. (1997). Such lower flux EGRET detections may be indicative of a quiescent gamma-ray flux or of gamma-ray flares that have no, or very low flux, radio-wave counterparts. These flares may be of the same type as the 1977 optical flare without a low-frequency counterpart. Comparisons between individual gamma-ray and radio-wave flares is difficult because of poor sampling and the highly variable character of blazars at all wavelengths.

We can associate the increased activity in the radio and gamma-ray bands. We see in Figure 2 that the rise in gamma-ray flux is correlated with the rise in flux from 8.0 to 90 GHz. The 4.8 GHz flux appears uncorrelated with the higher frequency activity. The correlation is particularly tight between the 90 GHz and gamma-ray flux. In Figure 4,

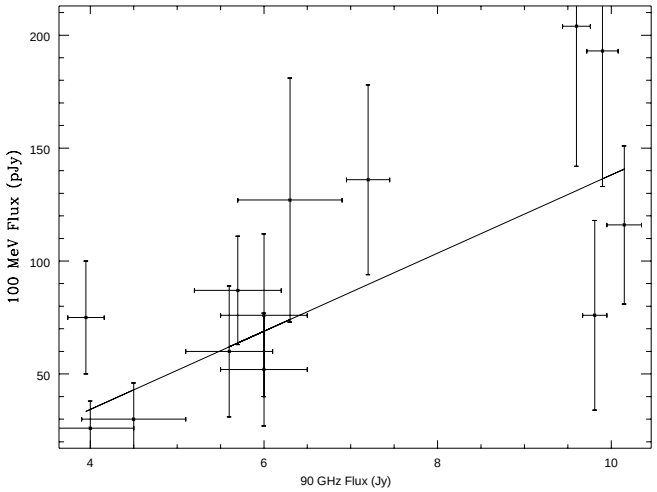

FIG. 4.—Scatter plot of 90 GHz vs. 100 MeV flux. The 90 GHz data are averaged over an 0.1 yr period centered on the gamma-ray detection. The line is a linear least-squares fit to the data.

we plot the average 90 GHz flux against the gamma-ray flux for 13 EGRET observations for which there were 90 GHz observations within 0.1 yr of the gamma-ray observation. The solid line indicates a least-squares fit to the data with a slope of 17.3 ± 4.0 pJy Jy^{-1}. The χ^2 of the fit is 11.5 for 11 degrees of freedom. Correlation with the gamma-ray flux at lower frequencies is enhanced with inclusion of a time delay.

This behavior is similar to that seen in 3C 279, with the exception that the correlated broadband activity extends to millimeter and centimeter wavelengths in NRAO 530 (Maraschi et al. 1994). Because of the sparse time sampling, the data are not sufficient to discriminate between models for the emission. Synchrotron self-Compton models, the pair cascade model (Levinson 1996), and external photon models (Sikora et al. 1994) can all produce contemporaneous synchrotron and gamma-ray flux increases.

We will discuss in § 3 VLBI observations that indicate that new jet components were created during the millimeter-wave flares. The correlation between millimeter and gamma-ray activity implies that the gamma-ray activity is associated with the VLBI component creation. Gamma-ray activity has also been associated with the creation of new VLBI components in 0528+134 (Pohl et al. 1995) and 3C 279 (Wehrle et al. 1996).

The opacity of X-ray to gamma-ray photons permits an estimate of the Doppler boosting factor, δ. Following Mattox et al. (1993), we find $\delta > 2.3[(T_{\rm var}/10^5\ {\rm s})(F_{1\ {\rm keV}}/0.2\ \mu{\rm Jy})^{-1}]^{-1/5}$. We take the 1 keV flux from the minimum observed for NRAO 530. We discuss X-ray observations of NRAO 530 and X-ray variability of blazars in detail in § 4.2. This result is sensitive to the power-law index of the X-ray energy spectrum, which we assume to be 0.5. J. Streiber (1996, private communication) reports the index to be 0.5 ± 0.5 for the case of fixed Galactic absorption and -0.5 ± 1.0 when absorption is a free parameter. Harder spectra produce higher lower limits for δ; for an index of -0.5, the lower limit is 7.5. The variability timescale for gamma rays, $T_{\rm var}$, is also poorly known. Von Montigny et al. (1995a) report values in the range 10^5–10^7 s. If NRAO 530 is evolving on a multiyear timescale, $T_{\rm var}$ may be on the order of 10^8 s.

3. VLBI OBSERVATIONS

3.1. *Observations and Calibration*

The VLBI observations were taken on 1995 April 25 and 26 with the array of Haystack Observatory, NRAO at Kitt Peak, and Hat Creek Radio Observatory under the auspices of the Coordinated Millimeter-VLB Array. The observing frequency was 86.243 GHz. Haystack and Hat Creek recorded left circular polarization with a bandwidth of 112 MHz; Kitt Peak recorded left circular polarization with a bandwidth of 56 MHz. Scans of 390 s were spaced 30 minutes apart.

The data were correlated with the Haystack Mk IIIA correlator. Coherent integration over periods longer than a few seconds decorrelated the signal significantly. Accordingly, we incoherently averaged over each scan with a coherence interval of 2 s (Rogers, Doeleman, & Moran 1995).

Hat Creek observed in its B array, which has a maximum baseline of 130 m. The antennas were phased together for each scan by observing the source for a few minutes and applying the self-calibrated phases as a phase offset to the local oscillator signal. Comparing the phases in the local correlator during the VLBI scan allowed us to estimate the scan average phasing efficiency. Near transit, the efficiency was as high as 90%. See Bower et al. (1997) for further details on array phasing.

On bright sources such as NRAO 530, errors in amplitude calibration are more significant than thermal noise. Kitt Peak and Hat Creek calibration factors were determined by measured values of the ratio of antenna to system temperature. The gain for Haystack was determined by the gain-elevation curve given in the Haystack Observatory guide, calibrated to match the measured antenna temperature for 3C 273B and 3C 279 at elevations near 40°, where the gain curve reaches a maximum. The estimated error from scan to scan in the amplitude gains is 10%, which we add in quadrature to the thermal error.

Phase noise added to the signal through unstable oscillators and other unstable components may also cause amplitude errors through decorrelation. At each site prior to the experiment a radio frequency test tone phase-locked to the maser was injected into the receiver. The signal was mixed to baseband by the oscillator chain and studied with a spectrum analyzer. At all stations, the phase noise was down by 30 dB or more, indicating that decorrelation due to instrumental phase noise was not significant. Phase noise in the maser and in the correlator is not tested by this experiment, however.

3.2. *Results*

We see distinct evidence for asymmetric structure in the 1995 April VLBI data. Our best-fit model (Table 2) for the total flux has four components that we identify as core, jet component 1 (C1), jet component 2 (C2), and halo. We show in Figure 5 an image of our best-fit model convolved with a beam 410×90 μas at a position angle of $-5\overset{\circ}{.}8$. Crosses indicate the positions of the core and the components C1 and C2.

We compare the amplitude visibilities and the closure phases with the model in Figure 6. The visibilities agree well from day to day. The amplitude data may be fit by a single component with a flux of 7 Jy and FWHM of 120 μas. However, the nonzero closure phase is a robust indicator of

TABLE 2

NRAO 530 Model Parameters: 1995 April

Component	Flux (Jy)	Size (μas)	Radius (μas)	Position Angle (deg)	T_b (K)
Core.....	3.7 ± 0.3	55 ± 30	...	...	$2.2 \pm 2.5 \times 10^{11}$
C2	1.7 ± 0.2	50 ± 65	95 ± 20	-107 ± 10	$1.2 \pm 3.5 \times 10^{11}$
C1	1.5 ± 0.2	110 ± 20	255 ± 35	-138 ± 10	$2.1 \pm 1.1 \times 10^{10}$
Halo	5.6 ± 1.3	> 900	...	...	$\lesssim 6.1 \times 10^{8}$

the need for multiple components. As a check against systematic errors in the closure phase, we determined that the closure phase of the blazar 3C 279 from contemporaneous observations did not deviate from zero and that the closure phase of the blazar 3C 273B from contemporaneous observations deviated from zero but with a different character. Three components are necessary to provide the change in the closure phase along with the essentially flat amplitudes. In addition, to match the model with the zero-baseline flux we require a resolved component, larger in scale than 900 μas. We identify this resolved component as the halo. Fits with more components did not substantially improve the χ^2 statistic and were rejected. Since the component C2 was not fully resolved from the core, the errors in its model characteristics are strongly correlated with those of the core.

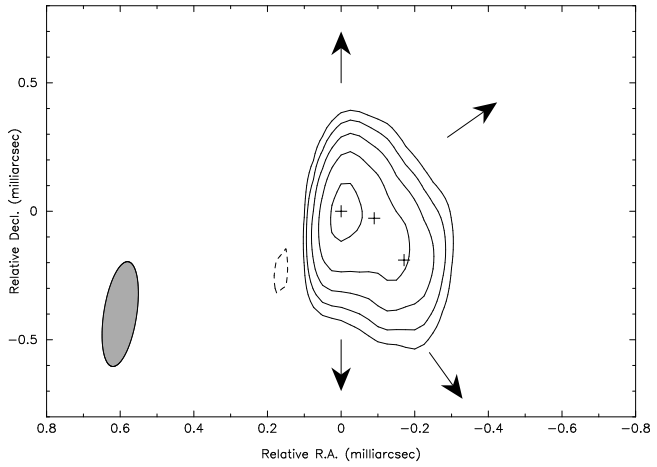

Fig. 5.—Image of NRAO 530 from the 86 GHz VLBI experiment in 1995 April. The crosses indicate the location of the core and components C1 and C2. The arrows point in the directions of components identified clockwise from north by Bondi et al. (1996), Zhang (private communication, 1995), Marscher & Broderick (1981), and Bondi et al. (1996). The beam is indicated in the lower left. Contour levels are -5, 5, 10, 20, 40, and 80% of the peak flux.

4. DISCUSSION

4.1. *Structure and Dynamics*

The 1995 April VLBI structure differs sharply from that of 3 mm wavelength VLBI observations obtained in 1994 April, prior to the flare. These observations, described in Rogers et al. (1994) and reanalyzed by Doeleman (1995), show a single component with $S = 3.88 \pm 0.08$ Jy and FWHM $= 85 \pm 10$ μas ($T_b = 8.8 \pm 2.3 \times 10^{10}$ K). Closure phases on the Haystack-Kitt Peak-Owens Valley triangle were consistent with zero. The observations also imply a halo of ~ 2 Jy greater than 2 mas in size.

We identify the brightest component of the 1995 April model as the core because of its similarity to the pre-outburst object and its location relative to the other components. However, without a spectral index, identification

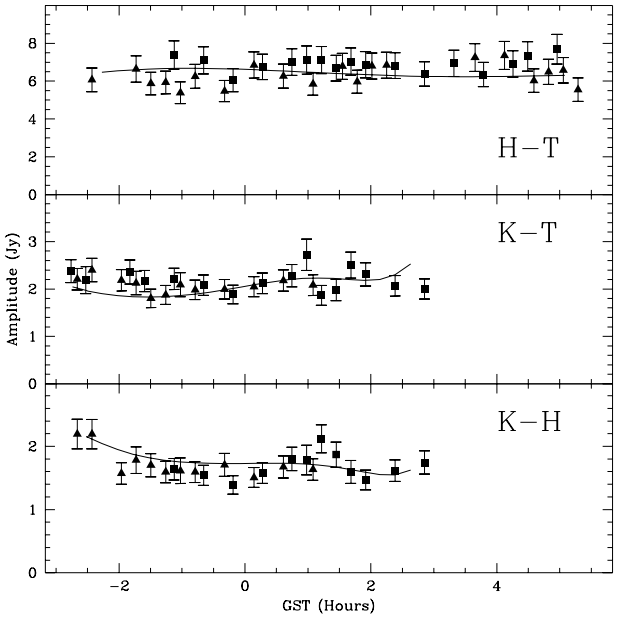

Fig. 6*a*

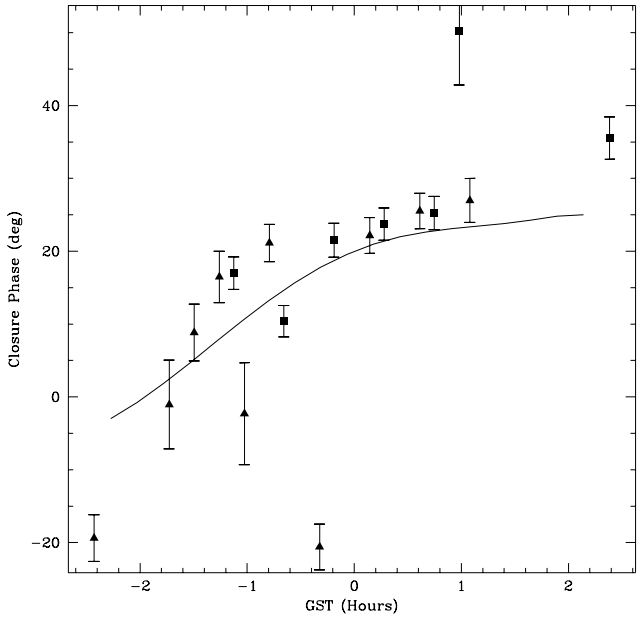

Fig. 6*b*

Fig. 6.—(*a*) Amplitude visibilities from the 1995 April VLBI experiment. The error bars indicate one standard deviation. Solid curves through the data are from the model in Table 2. K refers to Haystack, T to Kitt Peak, and H to Hat Creek. Data from 1995 April 25 are shown as solid squares. Data from 1995 April 26 are shown as solid triangles. (*b*) Closure phase from the 1995 April VLBI experiment on the Haystack-Hat Creek-Kitt Peak triangle. The error bars indicate one standard deviation.

of the core is imprecise. The similarity between the pre- and postoutburst cores suggests that the flare occurred outside or was rapidly ejected from the core.

The first jet component originates at a projected distance from the core of 0.4 h^{-1} pc or less. Unfortunately, our images are not of sufficient sensitivity to compare to the morphologies predicted by different gamma-ray emission models (Marscher 1995). We can calculate apparent velocities under the assumption that the jet components were ejected from the core. Based on the absence of VLBI structure in 1994 April, we estimate minimum apparent velocities $\beta_{\rm app}^{\rm C2} > 1.3\ h^{-1}$ and $\beta_{\rm app}^{\rm C1} > 3.2\ h^{-1}$ for the two components. More realistically, we associate the creation of the outer jet component (C1) with the first flare and the creation of the inner jet component (C2) with the second flare. Given the rapid transition from the second flare's peak at 1 mm to the peak at 3 mm and the likelihood of ejection at the time of the flare, we estimate that component ejection occurred no more than 0.2 yr prior to its apparent onset at 3 mm. We set ejection times at 1994.85 ± 0.2 and 1995.15 ± 0.2 yr and find apparent velocities $\beta_{\rm app}^{\rm C2} \gtrsim 7.9 \pm 4.3\ h^{-1}$ and $\beta_{\rm app}^{\rm C1} \approx 7.4 \pm 3.3\ h^{-1}$, respectively, consistent with uniform ejection at two epochs.

Similarly, we calculate apparent velocities for the halo. The increase in the flux of the halo from 1994 April to 1995 April requires an expanding component. The size implies $\beta_{\rm app} \gtrsim 26\ h^{-1}$ for material expanding from the onset of the first flare. The absence of structure in 1994 April requires $\beta_{\rm app} > 11.6\ h^{-1}$.

The position angles of the jet components are constrained well enough to indicate that a bend of $\sim 30°$ occurs in the jet between 100 and 250 μas away from the core. Lower frequency VLBI observations indicate bending on larger scales, as well. In Figure 5, we include arrows that point toward components detected in other experiments. Marscher & Broderick (1981) report a 2 Jy secondary component at 1.2 mas at a position angle of $-156°$ in their 2.8 cm wavelength map made from observations in 1980. Bondi et al. (1996) report on three epochs of 18 cm wavelength mapping between 1980 and 1988. They show a core of 2 to 5 Jy and two stationary knots of ~ 1 Jy each, one 25 mas directly north and one 20 mas directly south of the nucleus. Together, these data also suggest a bend with respect to the kiloparsec-scale structure. A VLA map at 8.4 GHz shows the jet exiting from the nucleus at a position angle of $-45°$ before it arcs to the location of the secondary at $-87°$ (J. Q. Zhang, private communication).

A single kink in the jet is not sufficient to account for the VLBI and large-scale observations. These observations are also not well fit by a low-pitch helical jet. This model, favored by Conway & Murphy (1993) for the creation of orthogonal misalignment between parsec- and kiloparsec-scale features, requires that the position angle changes monotonically from the small- to large-scale. To accommodate with a helical jet the range of position angles observed, a full turn or more on a cone with opening half-angle greater than the angle to the line of sight (or on a cylinder of a similar size at the distance of the 18 cm wavelength component) is necessary. That is, we require a jet viewed down its axis that winds one or more times around that axis within the inner 20 mas. Conway & Murphy (1993) discuss the pitfalls of such high-pitch helices, including the large size subtended by components and motion perpendicular to the axis of the cone at the location of maximum beaming.

Binary black holes (Begelman, Blandford, & Rees 1980) or hydrodynamic instability (Hardee 1987) are commonly cited as the source for helical motion in jets. Camenzind & Krockenberger (1992) argue in an alternative model that the rapidly rotating plasma near a rotating black hole will produce nonaxisymmetric bubbles that would appear to move in a helical pattern in the jet. The bubbles are collimated further downstream.

We note that if the observation of the southern component in 18 cm wavelength maps of Bondi et al. (1996) is spurious and the core is identified with component C1 in our image and with the southeastern component in the Marscher & Broderick (1981) image, then a simple low-pitch helical model can be roughly fit to the observations. Spurious symmetric features do arise in observations with limited u-v coverage. The helix would begin to the northwest and proceed through the northern 18 cm wavelength component and out the direction of the kiloparsec-scale component. The change in position angle between the innermost and outermost components would be 90°.

4.2. *Modeling the Synchrotron Emission*

We show in Figure 7 the spectrum of NRAO 530 at the time of the 1995 April experiment and a possible spectral decomposition. The spectrum is an interpolation of the two nearest spectra (H and J); error bars are expanded to account for variability. The core is assumed to have the quiescent spectrum. The two jet components are modeled as self-absorbed synchrotron sources with turnover frequencies of 15 and 60 GHz, optically thin spectra following $S_\nu \propto \nu^{-1}$, and peak flux densities of 10 Jy each. This decomposition is by no means unique; however, in addition to matching the spectrum and the VLBI characteristics, the decomposition is consistent with the predictions of Marscher & Gear (1985) for a shock in an inhomogeneous jet. In particular, the two jet components evolve in our

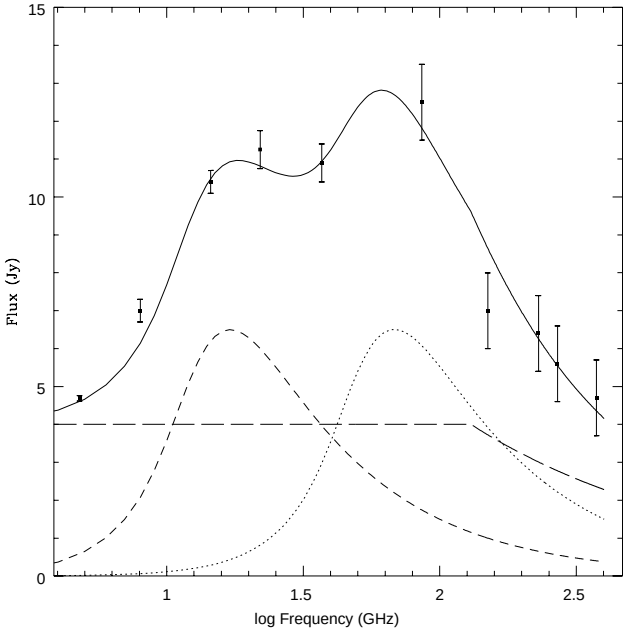

FIG. 7.—Spectrum at the time of the 1995 April experiment and a spectral decomposition. The long-dashed line indicates the model for the core. The medium-dashed line indicates the model for component C1. The short-dashed line indicates the model for component C2 and the halo. The solid line is the sum of all components.

model with nearly constant peak flux densities as the frequency of their peak flux densities decreases, a phenomenon that Marscher & Gear (1985) predict for sources in which synchrotron losses dominate.

The 15 GHz peaked component, associated with the earlier outburst, has an 86 GHz flux of 1.7 Jy, in agreement with the measured flux for C1. The 60 GHz peaked component, associated with the later outburst, has an 86 GHz flux of 6.1 Jy. We speculate that this component has two constituents: C2 with 1.7 Jy and the halo with 4.4 Jy. We note that the halo itself may be composed of two parts: one corresponding to the 1994 April excess flux and another corresponding to the recent flare. Making this distinction does not significantly affect our analysis.

With this decomposition we can estimate the physical conditions in each component. We first apply the inhomogeneous jet model of Königl (1981) to the flat-spectrum core. This model was created to describe the flat spectra seen in many radio cores. The model predicts the spectral indices, the frequency turnover, the peak flux density, the size, and the high-energy spectrum that results from an unresolved jet with a radial magnetic field ($B \propto r^{-m}$) and electron distribution ($N \propto \gamma_e^{-p} r^{-n}$), an opening angle ϕ, and a Doppler boosting factor δ at an angle to the line of sight θ. γ_e is the Lorentz factor for the internal electron energy of the jet. The general model is unconstrained. However, Königl (1981) makes a number of simplifying assumptions, which permits us to extract solutions given our model spectrum and VLBI component. Additionally, we assume the minimum electron Lorentz factor to be 100 (Wardle 1977). Two of the three parameters m, n, and p are constrained by the thin and thick spectral indices. The solutions are on two branches. If we assume $0.5 \leq n \leq 4$, we find one branch in the space bounded by $1.85 \leq m \leq 5.02$ and $1.05 \leq p \leq 1.90$. The second branch is in the space defined by $0.24 \leq m \leq 0.57$ and $-10.1 \leq p \leq -2.1$. Given the difficulty of creating the inverted spectrum of the latter branch, we assume that the parameters fall on the former branch. The flat to rising electron energy distribution this requires highlights the theoretical difficulties in creating a flat-spectrum source. We evaluate the magnetic field and the particle density at $r_0 = 0.2$ pc, the radius of maximum brightness temperature, with $\delta = \csc\ \theta = 10$. We find $B = 2$G and the particle density in the range 1 to 2×10^3 cm^{-3}. The opening angle $\phi \approx 0.01$ rad. If the jet continues to open at this angle, it will be comparable to the deprojected angles subtended by the jet components. Such a small opening angle is probably inconsistent with the hypothesis of a fully rotating helical jet matching our observations.

We next analyze the jet and halo components in terms of standard synchrotron theory for relativistic components (Marscher 1983). We assume again the minimum electron Lorentz factor to be 100. We show the results in Table 3. The models for C2 and C1 are consistent with the core model. The timescale for synchrotron cooling at 86 GHz for $B = 1$ G and $\delta = 10$ is 0.3 yr, which is also consistent with the spectral evolution in our model.

TABLE 3

SYNCHROTRON MODEL PARAMETERS

Component	Magnetic Field (G)	Particle Density (cm^{-3})
C2	1	0.01
C1	0.002	300
Halo	18000	6×10^{-10}

The halo model, however, requires a field and a particle density sharply different from the parameters of the other models. These extreme values are caused by the high peak frequency for the halo. However, a lower peak frequency will significantly degrade the fit to the spectrum. This poor fit and the required large size of the halo suggest that the halo may be formed through a different process. For instance, the collision of an ejected component with the local medium might excite a larger area at a lower brightness temperature. Collisions of this kind could occur on the edge of the jet or at a bend in the jet. We can reconcile the apparent velocity of the halo with that of the components C1 and C2 if we assume that the halo material was ejected at an earlier epoch but did not radiate synchrotron photons until the halo material collided with the local medium or experienced a change in the jet conditions. Such a model requires a coincidence in the timescales for the halo and the jet components to reach maximum brightness that appears improbable.

Both the core and jet models predict that synchrotron photons will scatter through the inverse-Compton process to higher energies. Component C1 dominates at $E_\gamma = 1$ keV with a predicted flux of $10\delta^{-6}$ Jy. NRAO 530 has been observed with the *Einstein* IPC in 1979 to have a 1 keV flux of 0.2 μJy (Marscher & Broderick 1981) and during the *ROSAT* all-sky survey in 1990 and 1991 to have a 1 keV flux of 0.63 μJy (Brinkmann, Siebert, & Boller 1994). Unfortunately, neither of these observations are contemporaneous with the recent flare. We estimate an upper limit to the flux based on the variability of other blazars. McNaron-Brown et al. (1995) found that all blazars detected with OSSE in the energy range 50 to 150 keV showed variability by a factor of 3 on a timescale of months. Giommi et al. (1990) studied variability of BL Lac objects in archived *EXOSAT* soft and hard X-ray data. They found luminosity variability with amplitudes from 10% to a factor of 30 over timescales of minutes to years. Most sources varied by less than a factor of 10. They found no evidence for secular variations. We set a factor of 10 as the upper limit to 1 keV variability in NRAO 530, implying $\delta > 11(F_{1\ \mathrm{keV}}/6\ \mu\mathrm{Jy})^{-1/6}$. This value is significantly greater than that of Marscher & Broderick (1981), who calculate $\gamma \gtrsim 2$. This may indicate a period of heightened activity in the present epoch.

4.3. *Polarization*

The history of the centimeter wavelength polarization is complex. We show the polarized flux fraction in Figure 8 and the polarization position angle in Figure 9 at 4.8, 8.0, and 14.5 GHz. In particular, we see slow change in the polarization position angle, χ, punctuated by dramatic jumps. Prior to 1978, χ rose at a rate barely indistinguishable from zero. From 1978 to the early 1990s, χ declined at an average rate of 5° yr^{-1}. A sharp reversal took place then, the time and magnitude of which were frequency-dependent. At 14.5 GHz, the reversal began in 1993 and was more than 90°. At 4.8 GHz, the reversal began in 1991 and was $\sim$60°. The frequency dependence of the reversal created a change in the rotation measure, from -45 ± 10 rad m^{-2} to $+44 \pm 10$ rad m^{-2}. Similar but briefer reversals occurred prior to 1990. From 1994 to the present, χ has neither risen nor declined substantially, and the rotation

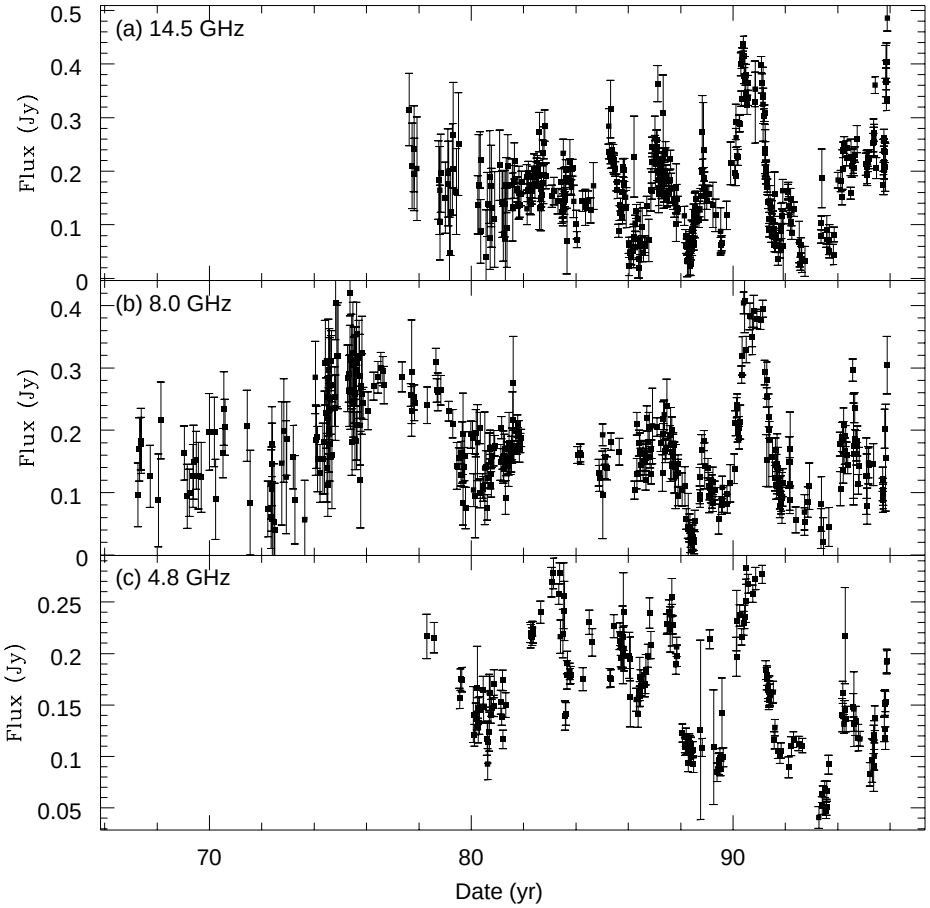

FIG. 8.—Polarized flux at (*a*) 14.5 GHz, (*b*) 8.0 GHz, and (*c*) 4.8 GHz from the University of Michigan

measure has decreased to -90 ± 20 rad m^{-2}. The rotation measures before and after the reversal agree with the value of -63 ± 5 rad m^{-2} (Rusk 1988).

The slow, linear change in χ from 1975 to 1990 is characteristic of the rotator phenomenon described by Aller, Hodge, & Aller (1981). These authors consider a rotating magnetic field to be the likely source for both the slow and rapid change in χ. Jones et al. (1985) point out that such events may occur as the result of a random walk in Stokes $Q - U$ space generated by a turbulent magnetic field.

The reversal in the 1990s may be associated with a flare that peaked at centimeter wavelengths in 1990. This flare was accompanied by a sharp increase in the polarization fraction. As Hughes, Aller, & Aller (1985) demonstrate, a shock in a jet will generate an increase in the polarized flux fraction because of the compression of magnetic field in the shock. The position angle swings from that of the ambient jet to that of the shocked component. Frequency-dependent opacity will lead to the apparent change in the rotation measure. Faraday rotation is an unlikely source for this change since we expect a larger effect at longer wavelengths. We note that for properly tuned parameters, small changes in the jet parameters will also lead to dramatic changes in the polarization position angle, simply as a consequence of the geometry (Blandford & Königl 1979).

We apply the rotation measure to the centimeter wavelength position angles to estimate the position angle at 86 GHz as $90° \pm 10°$ in 1995 April. The magnetic field is therefore nearly perpendicular to the jet axis at its base but askew by $\sim 45°$ at the component C1. This is consistent with the hypothesis that the change in position angle is driven by a transverse shock at the base of the jet.

5. GAMMA-RAY BLAZARS

Our findings are similar to those of other studies of gamma-ray blazars. Superluminal motion is common to all sources with sufficient statistics. Barthel et al. (1995) summarize previous identifications of superluminal motion in eight sources and provide evidence of superluminal motion in 1633+382. Recently, superluminal motion has also been identified in 0528+134 (Pohl et al. 1995), 0420−014 (Wagner et al. 1995), and 0521−365 (Tingay et al. 1996). In addition, gamma-ray emission was detected from two already known superluminal sources: 1101+384 (Bååth & Zhang 1991) and 1222+216 (Hooimeyer et al. 1992b). 1156+295 has also been identified as an EGRET source. However, as Vermeulen & Cohen (1994) note, its apparent velocity is quite uncertain. With our identification of superluminal motion in NRAO 530, the number of EGRET sources with confirmed superluminal motion is now 15.

Many sources also exhibit a parsec-scale jet that is bent or is misaligned with the kiloparsec-scale jet. We summarize in Table 4 the results of a survey of the literature for jet position angle information on sources taken from the Second EGRET Catalog (Thompson et al. 1995). In column (2), certain EGRET identifications are marked with an A; marginal EGRET identifications with an a. The VLBI data, which range in wavelength from 18 cm to 3 mm, are not an

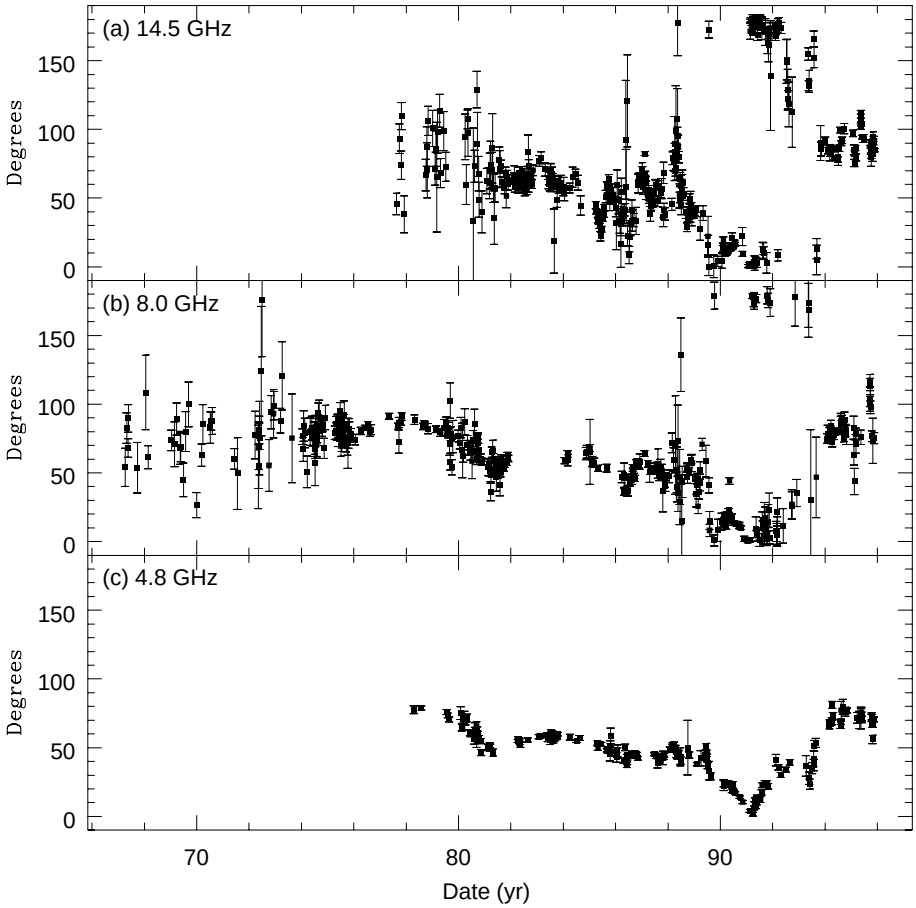

FIG. 9.—Polarization position angle at (*a*) 14.5 GHz, (*b*) 8.0 GHz, and (*c*) 4.8 GHz from the University of Michigan

exhaustive summary. Instead, they are representative of the literature. Where a map but no value for the position angle was given, we chose the nearest octant for the position angle.

We show in Figure 10 a histogram of the largest observed misalignment angle between the parsec- and kiloparsec-scale structure for the 28 EGRET sources for which both position angles are available. For the two sources in which two secondary kiloparsec-scale structures are apparent, we add 0.5 to the bins for each misalignment angle. The distribution is peaked at small misalignment angle with some evidence for a secondary peak at 90°. The distribution is not fit by a uniform distribution ($\chi_\nu^2 = 3.0$). We compare our distribution with the distributions of Xu et al. (1994) for the Caltech-Jodrell Bank snapshot survey and the Pearson-Readhead survey, excluding from our sample the six EGRET sources that appear in the Xu et al. (1994) sample. The distribution for all sources and the distribution for high optical polarization sources agree equally well with our distribution ($\chi_\nu^2 = 0.7$). However, the distribution for low optical polarization sources is more discrepant ($\chi_\nu^2 = 1.4$). We see no significant change if we exclude EGRET sources with marginal detections from our sample. Although the optical polarizations of the EGRET sources are typically high, we note the presence of several low-polarization sources including 0528+134, 3C 273B, and 1611+343 (Impey & Tapia 1990). The geometry of gamma-ray blazars is apparently similar to that of other blazars, including both high- and low-polarization objects. This contradicts the conclusion of von Montigny et al. (1995b), which was based on a smaller number of sources, that a difference in the curvature of the jets of gamma-ray–loud and gamma-ray–quiet objects exists. The small number of sources and the uneven nature of the sample make these conclusions tenta-

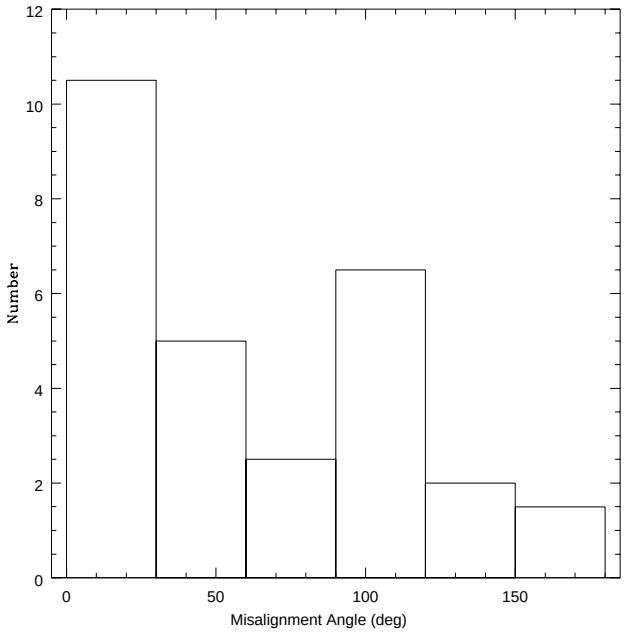

FIG. 10.—Misalignment angle between the parsec- and kiloparsec-scale structure based on a survey of the literature. References are given in Table 4.

TABLE 4

PARSEC- AND KILOPARSEC-SCALE POSITION ANGLES OF JETS IN EGRET BLAZARS

Name (1)	ID (2)	P.A.—kpc (deg) (3)	Reference (4)	P.A.—pc (deg) (5)	λ (cm) (6)	Reference (7)
0130−171	a	…	…	…	…	…
0202+149	A	unres	1	285	18	2
0208−512	A	233	3	233	6	3
0219+428	a	…	…	…	…	…
0235+164	A	−69, 25	4	6–47	6	5
				6	1.3	5
0234+285	a	NW	6	N, NE	3.8	6
0420−014	A	NE, S	7	178–240	3.6	8
0446+112	A	270, 210	1	…	…	…
0458−020	a	SW	9	−55	3.8	6
0521−365	A	310	3	310	3.5, 6	3
0528+134	A	N	1	6–83	1.3	10
				33–88, 286	1.3	11
				13–44, 237–297	3.6	11
0537−441	A	305	1	3	3.5, 6	3
0716+714	A	−60	1	17	18	12
				7	6	13
0735+178	A	170	1	40–80	6	14
				26–110	1.3	15
0804+499	a	199	4	142	18	12
0805−077	a	…	…	…	…	…
0829+046	A	…	…	…	…	…
0827+243	A	200	1	141	2.8	16
0836+710	A	200	1	214–220	6	17
0917+449	a	270	1	199–221	18	12
				176–198	6	13
0954+556	A	300, 50	1	…	…	…
0954+658	A	205	1	263–303	6	18
1101+384	A	315	19	288	1.3	15
				315	6	19
				307–336	6	13
1127−145	A	41	6	10–30	18	2
				NE, E	3.8	6
1156+295	A	340	1	20–50	18	20
				10–90	6	20
				NE	1.3, 2.8	20
1222+216	A	345	21	345	6	21
1226+023	A	222	1	223–245	6	22
1229−021	A	…	…	…	…	…
1253−055	A	4.7, 202	1	225	1.3, 2.8, 6	23
1317+520	a	134	24	125	6	13, 24
1313−333	a	…	…	…	…	…
GRO J1314−42	a	51	25	51	3.6, 13	25
1331+170	A	…	…	…	…	…
1406−076	A	…	…	…	…	…
1510−089	A	160	1	…	…	…
1604+159	A	…	…	…	…	…
1606+106	A	W	4	…	…	…
1611+343	A	303, 90	1	…	…	…
1622−253	A	…	…	…	…	…
1633+382	A	168	4	290–318	6	26
				115, 297	6	17
1730−130	A	273	1	204	2.8	27
				222–253	0.3	28
				0, 180	18	2
1739+522	A	260	1	9	18	12
1908−201	A	…	…	…	…	…
1933−400	A	140	1	…	…	…
2022−077	A	…	…	…	…	…
GRO J2039+11	a	…	…	…	…	…
2052−474	A	…	…	…	…	…
2209+236	A	…	…	…	…	…
2230+114	A	140	1	157	6	29
2251+158	A	318	1	265	1.3, 2.8	30
				295–307	18	30
2356+196	A	…	…	…	…	…

NOTE.—Col. (1): Source name; col. (2): EGRET identification status: A = AGN, a = AGN (marginal); col. (3): Position angle measured on the kiloparsec scale; col. (4): Reference for col. (3); col. (5): Position angle measured on the parsec scale; col. (6): Wavelength in cm of the parsec position angle measurement; col. (7): Reference for cols. (5) and (6).

REFERENCES.—(1) Perley 1982; (2) Bondi et al. 1996; (3) Tingay et al. 1996; (4) Murphy, Browne, & Perley 1993; (5) Chu et al. 1996; (6) Wehrle et al. 1992; (7) Antonucci & Ulvestad 1985; (8) Wagner et al. 1995; (9) Briggs et al. 1989; (10) Pohl et al. 1995; (11) Zhang et al. 1994; (12) Polatidis et al. 1995; (13) Xu et al. 1995; (14) Bååth & Zhang 1991; (15) Zhang & Bååth 1991; (16) Marscher & Broderick 1983; (17) Pearson & Readhead 1988; (18) Gabuzda et al. 1994; (19) Zhang & Bååth 1990; (20) McHardy et al. 1990; (21) Hooimeyer et al. 1992b; (22) Unwin et al. 1985; (23) Unwin et al. 1989; (24) Hooimeyer et al. 1992a; (25) Jones et al. 1996; (26) Barthel et al. 1995; (27) Marscher & Broderick 1981; (28) This paper; (29) Wehrle & Cohen 1989; (30) Pauliny-Toth et al. 1987.

tive. Further, the observed degree of bending or misalignment may be a strong function of observing frequency; the broad wavelength range of our sample may blur features in the distribution.

While superluminal motion and bent or misaligned jets are common, the case of the gamma-ray–quiet 3C 345, with its well-documented bent, relativistic jet (e.g., Unwin et al. 1994) makes the argument against sufficiency for both criteria. In addition, many of the superluminal sources of Vermeulen & Cohen (1994) and many of the misaligned sources in Xu et al. (1994) have not been detected with EGRET. This point must be tempered with an awareness of the sparse sampling of EGRET and the long timescales for variability, which the history of NRAO 530 amply illustrates.

6. CONCLUSIONS

We have shown that the recent radio and millimeter wavelength flare in the blazar NRAO 530 is a unique event in its 30 yr history. This flare may be associated with higher excitation in the source that began as early as 4 yr prior to the flare's peak. Evidence for an increase in activity in the 4 yr prior to the flare includes an increase in gamma-ray flux and the reversal of a decades-long trend in the polarization position angle. This is supported by the increase in the minimum jet Lorentz factor between 1980 and 1995 inferred from synchrotron self-Compton models.

Our VLBI observations indicate the creation of new components in a bent, highly beamed jet coincident with the flare. Our estimates for the apparent velocity of the jet components and Doppler boosting factors from synchrotron self-Compton and gamma-ray opacity models require a jet with an angle to the line of sight less than 0.1 rad and a bulk Lorentz factor greater than 10. The same analysis for the halo constrains the angle to the line of sight similarly but requires a significantly greater Lorentz factor. The large size of the halo poses a problem that we are unable to resolve. Further VLBI observations with a wider field of view are necessary to identify the size and location of this component. We plan high-frequency VLBI observations and broadband monitoring in order to investigate the jet conditions more deeply.

Further high-frequency VLBI imaging of gamma-ray–loud and gamma-ray–quiet blazars is also necessary. In our survey of the literature, we identified VLBI maps for 29 of the EGRET sources and many of those only at low frequencies. Reliable apparent velocities are available for less than one-third of the sample. High-frequency imaging is necessary to test fully the hypothesis that gamma-ray emission does originate in relativistic jets aligned with the line of sight and to search for systematic differences between the gamma-ray–loud and gamma-ray–quiet populations. These differences may appear in the dynamics, morphology, or environment of blazars. Broadband monitoring from the radio to the gamma-ray spectrum will also play a crucial role in this effort.

We emphasize the need for VLBI at frequencies where the emission is optically thin. With sufficient sensitivity, these images can discriminate between different models of gamma-ray emission (Marscher 1995). Improved sensitivity at high frequencies can be achieved through instrumental and technical advances, including the installation of 3 mm wavelength receivers on VLBA antennas and the implementation of techniques for correction of atmospheric phase fluctuations (Bower et al. 1997).

We thank the staffs of Haystack, Kitt Peak, and Hat Creek observatories for their assistance with VLBI. We are grateful to J. Carlstrom, R. C. Hartman, E. I. Robson, J. Stevens, J. Streiber, H. Teräsranta, M. Tornikoski, and J. Q. Zhang for sharing data. We thank an anonymous referee for useful comments. This work was supported by National Science Foundation grants including AST 94-21979 and AST 93-07913. The Coordinated mm-VLBI Array Project is supported under a grant from the National Science Foundation to the NEROC Haystack Observatory. The National Radio Astronomy Observatory is a facility of the National Science Foundation operated under cooperative agreement by Associated Universities, Inc. The James Clerk Maxwell Telescope is operated by the Joint Astronomy Centre in Hilo, Hawaii on behalf of the parent organizations PPARC in the United Kingdom, the National Research Council of Canada, and the Netherlands Organization for Scientific Research. The NASA/IPAC extragalactic database (NED) is operated by the Jet Propulsion Laboratory, California Institute of Technology, under contract with the National Aeronautics and Space Administration. G. C. B. acknowledges the support of the Berkeley Graduate Fellowship.

REFERENCES

Aller, H. D., Aller, M. F., Latimer, G. E., & Hodge, P. E. 1985, ApJS, 59, 513
Aller, H. D., Hodge, P. E., & Aller, M. F. 1981, ApJ, 248, L5
Antonucci, R. R. J., & Ulvestad, J. S. 1985, ApJ, 294, 158
Bååth, L. B., & Zhang, F. J. 1991, A&A, 243, 328
Barthel, P. D., et al. 1995, ApJ, 444, L21
Begelman, M. C., Blandford, R. D., & Rees, M. J. 1980, Nature, 287, 307
Blandford, R. D., & Königl, A. 1979, ApJ, 232, 34
Bondi, M., et al. 1996, A&A, 308, 415
Bower, G. C., et al. 1997, J. Geophys. Res., in press
Briggs, F. H., et al. 1989, ApJ, 341, 650
Brinkmann, W., Siebert, J., & Boller, T. 1994, A&A, 281, 355
Camenzind, M., & Krockenberger, M. 1992, A&A, 255, 59
Chu, H. S., et al. 1996, A&A, 307, 15
Conway, J. E., & Murphy, D. W. 1993, ApJ, 411, 89
Doeleman, S. S. 1995, Ph.D. thesis, MIT
Duncan, W. D., Robson, E. I., Ade, P. A. R., Griffin, M. J., & Sandell, G. 1990, MNRAS, 243, 126
Fichtel, C. E., et al. 1994, ApJ, 434, 557
Gabuzda, D. C., Mullan, C. M., Cawthorne, T. V., Wardle, J. F. C., & Roberts, D. H. 1994, ApJ, 435, 140
Giommi, P., Barr, P., Garilli, B., Maccagni, D., & Pollock, A. M. T. 1990, ApJ, 356, 432
Hardee, P. E. 1987, ApJ, 318, 78
Hooimeyer, J. R. A., et al. 1992a, A&A, 261, 18
Hooimeyer, J. R. A., et al. 1992b, A&A, 261, 5
Hughes, P. A., Aller, H. D., & Aller, M. F. 1985, ApJ, 298, 301
Impey, C. D., & Tapia, S. 1990, ApJ, 354, 124
Jones, D. L., et al. 1996, ApJ, 466, L63
Jones, T. W., et al. 1985, ApJ, 290, 627
Junkkarinen, V. 1984, PASP, 96, 539
Königl, A. 1981, ApJ, 243, 700
Kühr, H., et al. 1981, A&AS, 45, 367
Levinson, A. 1996, ApJ, 459, 520
Maraschi, L., et al. 1994, ApJ, 435, L91
Marscher, A. P. 1983, ApJ, 264, 296
———. 1995, Proc. Natl. Acad. Sci., 92, 11439
Marscher, A. P., & Broderick, J. J. 1981, ApJ, 249, 406
———. 1983, AJ, 88, 759
Marscher, A. P., & Gear, W. K. 1985, ApJ, 298, 114
Mattox, J. R., et al. 1993, ApJ, 410, 609
McHardy, I. M., et al. 1990, MNRAS, 246, 305
McNaron-Brown, K., et al. 1995, ApJ, 451, 575
Mukherjee, R., et al. 1997, ApJ, submitted
Murphy, D. W., Browne, I. W. A., & Perley, R. A. 1993, MNRAS, 264, 298
Nolan, P. L., et al. 1996, ApJ, 459, 100

Pauliny-Toth, I. I. K., et al. 1987, Nature, 328, 778
Pearson, T. J., & Readhead, A. C. S. 1988, ApJ, 328, 114
Perley, R. A. 1982, AJ, 87, 859
Pohl, M., et al. 1995, A&A, 303, 383
Polatidis, A. G., et al. 1995, ApJS, 98, 1
Reich, W., et al. 1993, A&A, 273, 65
Rogers, A. E. E. 1994, Workshop on the Coordination of Millimeter VLBI (Westford: Haystack Obs.)
Rogers, A. E. E., et al. 1994, ApJ, 434, L59
Rogers, A. E. E., Doeleman, S. S., & Moran, J. M. 1995, AJ, 109, 1391
Rusk, R. E. 1988, Ph.D. thesis, Univ. Toronto
Sandell, G. 1994, MNRAS, 271, 75
Sikora, M., Begelman, M. C., & Rees, M. J. 1994, ApJ, 421, 153
Stevens, J. A., et al. 1994, ApJ, 437, 91
Stevens, J. A., & Robson E. I. 1994, MNRAS, 270, L75
Teräsranta, H., et al. 1992, A&AS, 94, 121
Thompson, D. J., et al. 1995, ApJS, 101, 259
Tingay, S. J., et al. 1996, ApJ, 464, 170
Tornikoski, M., et al. 1994, A&A, 289, 673
Tornikoski, M., et al. 1996, A&AS, 116, 157
Unwin, S. C., et al. 1985, ApJ, 289, 109
Unwin, S. C., et al. 1989, ApJ, 340, 117
Unwin, S. C., et al. 1994, ApJ, 432, 103
Valtaoja, E., & Teräsranta, H. 1995, A&A, 297, L13
Vermeulen, R. C., & Cohen, M. H. 1994, ApJ, 430, 467
von Montigny, C., et al. 1995a, ApJ, 440, 525
von Montigny, C., et al. 1995b, A&A, 299, 680
Wagner, S. J., et al. 1995, A&A, 298, 688
Wardle, J. F. C. 1977, Nature, 269, 563
Webb, J. R., et al. 1988, AJ, 95, 374
Wehrle, A. E., & Cohen, M. 1989, ApJ, 346, L69
Wehrle, A. E., et al. 1992, ApJ, 391, 589
Wehrle, A. E., et al. 1996, ASP Conf. Ser. 110, Blazar Continuum Variability, ed. H. R. Miller & J. R. Webb (San Francisco: ASP), 430
Welch, W. J., & Spinrad, H. 1973, PASP, 85, 456
Xu, W., Readhead, A. C. S., Pearson, T. J., Polatidis, A. G., & Wilkinson, P. N. 1995, ApJS, 99, 297
Xu, W., Readhead, A. C. S., Pearson, T. J., Wilkinson, P. N., & Polatidis, A. G. 1994, in Proc. NRAO Workshop 23, Compact Extragalactic Radio Sources, ed. J. A. Zensus & K. I. Kellermann (Green Bank: NRAO), 7
Zhang, F. J., & Bååth, L. B. 1990, A&A, 236, 47
———. 1991, MNRAS, 248, 566
Zhang, Y. F., et al. 1994, ApJ, 432, 91